Effective mass of omega meson and $NN\omega$ interaction at finite temperature and density

Song Gao
Department of Physics, Fudan University, Shanghai 200433, People's Republic of China

Ru-Keng Su
China Center of Advanced Science and Technology (World Laboratory), P.O. Box 8730, Beijing, People's Republic of China and Department of Physics, Fudan University, Shanghai 200433, People's Republic of China

Peter K. N. Yu
Department of Applied Science, City Polytechnic of Hong Kong, Kowloon Tong, Kowloon, Hong Kong
(Received 28 June 1993)

By means of the thermofield dynamical theory, the effective mass of omega meson is calculated by summing the bubble diagrams. It is found that the formula for the effective mass of the ρ meson can also be used to describe the ω meson in the low density region, but the parameter n and the critical temperature T_c depend on the density. The temperature and density dependence of one omega exchange potential of nucleon-nucleon interaction are given. The conjecture of Brown and Rho about the effective masses of mesons is discussed.

PACS number(s): 21.30.+y, 13.75.Cs

I. INTRODUCTION

It is widely believed that in future experiments nuclear systems will be investigated under extreme conditions of high temperature and/or high density. The heavy-ion collision experiments provide us with an opportunity to study the chiral phase transition as well as the quark deconfining phase transition. Much theoretical effort [1–12] is being devoted to the studies of physics under extreme conditions.

For studying the phase transition and the thermodynamical properties of the nuclear system under extreme conditions, it is essential to determine the temperature and density dependence of nuclear force. As is well known, the nuclear force can be understood on the basis of the exchange of various mesons. In a series of our previous papers [7–10], by using the Green's-function methods, we extended the one-pion-exchange potential with pseudoscalar and pseudovector couplings to finite temperature and finite density. At large distances, the exchange of the pion meson gives the dominant contribution to the NN force. However, at small distances, the dominant contributions of the nucleon-nucleon interaction is believed to be coming from the exchange of ω and ρ mesons. Therefore, it is of interest to extend our previous investigations to the $NN\omega$ interaction. In this paper, by employing the thermofield dynamical theory [13,14] and summing the bubble diagrams [7–10], which give the vacuum polarization of the $NN\omega$ interaction, we will calculate the effective mass of ω meson and the temperature and density dependence of nuclear force at small distances by exchanging one ω meson. This is the first objective of the present paper.

The second objective of the present paper is to check the conjecture of Brown and Rho [1,2] from another point of view. Based on QCD sum rules and the scale property of the Skyrmion model, Brown and Rho [2] argued that the effective masses of ρ, σ, and ω mesons and nucleons satisfy

$$\frac{M_\sigma^*}{M_\sigma} \simeq \frac{M_N^*}{M_N} \simeq \frac{M_\rho^*}{M_\rho} \simeq \frac{M_\omega^*}{M_\omega} , \tag{1}$$

where the masses with asterisks stand for the finite-temperature and finite-density values, and the effective mass of a ρ meson for a fixed density is

$$\frac{M_\rho^*}{M_\rho} = \left[1 - \left(\frac{T}{T_c}\right)^2\right]^n , \tag{2}$$

where T_c is the transition temperature at which M_ρ^* is zero, n is a constant, and $\frac{1}{6} \leq n \leq \frac{1}{2}$. Recently, many workers have checked the Brown-Rho conjecture from QCD arguments [15,16]. Instead of using QCD arguments, we hope to check Eqs. (1) and (2) from nucleon-nucleon-meson interactions. Based on the $NN\omega$ interaction, and the finite temperature and density quantum field theory, we can find M_ω^*/M_ω and check whether it can be described by Eq. (2). We will prove that for a fixed density, M_ω^*/M_ω can well be described by Eq. (2) in low-density regions, i.e., $\rho \leq 4\rho_0$, where ρ_0 is the saturation density. However, for high-density regions where $\rho > 4\rho_0$, it deviates from the description of Eq. (2), which means that the Brown-Rho conjecture in high-density regions may be incorrect.

II. FORMALISM

A. The Feynman propagator in thermofield dynamics

Our calculations are based on the framework of thermofield dynamics (TFD) [13,14], which has been employed by many authors for discussing different problems.

Contrary to the Matsubara imaginary time Green's-function method, TFD is formulated with the real-time variable from the beginning. In this theory, the ground state is identified as the temperature dependent vacuum. All ensemble averages are calculated as expectation values in this vacuum, and all operator formalism at zero temperature can be extended to finite temperature in a straightforward way.

In TFD, each field has double components, and they lead to a 2×2 matrix propagator. For example, the Feynman propagator of fermion field in TFD is

$$iS_F(k) = \begin{pmatrix} i\Delta_{11}(k) & i\Delta_{12}(k) \\ i\Delta_{21}(k) & i\Delta_{22}(k) \end{pmatrix} , \tag{3}$$

where

$$\Delta_{11}(k) = (\not{k} + M)\left(\frac{1}{k^2 - M^2 + i\varepsilon} + 2\pi i[\theta(k_0)n_F(k) + \theta(-k_0)\bar{n}_F(k)]\delta(k^2 - M^2)\right)$$
$$= -\Delta_{22}^*(k) , \tag{4a}$$

$$\Delta_{12}(k) = 2\pi i(\not{k} + M)e^{-\beta\mu/2}[\theta(k_0)e^{\beta(|k_0|-\mu)}n_F(k) - \theta(-k_0)e^{\beta(|k_0|+\mu)}\bar{n}_F(k)]\delta(k^2 - M^2)$$
$$= -e^{-\beta\mu}\Delta_{21}(k) , \tag{4b}$$

where $\not{k} \equiv \gamma^\mu k_\mu$, $\theta(k_0)$ is the step function, $n_F(k)$ and $\bar{n}_F(k)$ are, respectively, the fermion distribution and antifermion distribution given by

$$n_F(k) = \frac{i}{e^{\beta(|k_0|+\mu)} + 1} ,$$
$$\bar{n}_F(k) = \frac{1}{e^{\beta(|k_0|-\mu)} + 1} , \tag{5}$$

and $\beta = T^{-1}$ is the inverse of the temperature, where we have chosen $k_B = 1$. The chemical potential μ is determined by

$$\rho = \frac{\gamma}{(2\pi)^3}\int d^3k[n_F(k) - \bar{n}_F(k)] . \tag{6}$$

For a nucleon system, $\gamma = (2S + 1)(2\tau + 1) = 4$ is the spin-isospin degeneracy.

B. The effective mass of ω meson

Now we proceed to discuss the effective mass of ω meson at finite temperature and finite density. The Lagrangian density for $NN\omega$ interaction is

$$\mathcal{L}_I = -g_\omega\bar{\psi}\gamma^\mu\psi\omega_\mu , \tag{7}$$

where ψ and ω_μ are the nucleon field and ω meson field, respectively, and g_ω is the $NN\omega$ coupling constant. At zero temperature, the self-energy of vacuum polarization for ω meson under the bubble diagrams approximation (Fig. 1) is

$$\Sigma_\omega^{\mu\nu}(q,0) = ig_\omega^2\int\frac{d^4k}{(2\pi)^4}\mathrm{Tr}[\gamma^\mu S(k)\gamma^\mu S(k-q)] , \tag{8}$$

where $S(k)$ is the propagator of nucleon field at zero temperature. The Dyson equation for ω meson propagator can be written as

$$D_{\mu\nu}(q) = D^0_{\mu\nu}(q) + D^0_{\mu\nu}\Sigma_\omega^{\lambda\sigma}D_{\sigma\nu}(q) , \tag{9}$$

where

$$D^0_{\mu\nu}(q) = \left(-g_{\mu\nu} + \frac{q_\mu q_\nu}{M_\omega^2}\right)\frac{1}{q^2 - M_\omega^2 + i\varepsilon} \tag{10}$$

is the free propagator of the ω meson. The self-energy given by Eq. (8) can be written as

$$\Sigma_\omega^{\mu\nu}(q,0) = \left(g^{\mu\nu} - \frac{q^\mu q^\nu}{q^2}\Sigma(q)\right) . \tag{11}$$

From the Dyson equation (9), and from Eqs. (10) and (11), we have obtained [5] that

$$D_{\mu\nu}(q) = \left(-g_{\mu\nu} + \frac{q_\mu q_\nu}{q^2}\right)\frac{1}{q^2 - M_\omega^2 + \Sigma(q)}$$
$$-\left(\frac{q_\mu q_\nu}{q^2} - \frac{q_\mu q_\nu}{M_\omega^2}\right)\frac{1}{q^2 - M_\omega^2 + i\varepsilon} . \tag{12}$$

We now extend our discussions to finite temperature and finite density. According to the calculation rules of TFD, the finite-temperature and finite-density self-energy of the ω meson can be obtained by summing the same diagrams but replacing the Feynman propagator $S(k)$ by $\Delta_{11}(k)$ [13,14]. It can be proved that the diagonal matrices Δ_{11} of Eq. (3) alone is sufficient for the determination of the self-energy. Therefore, we have

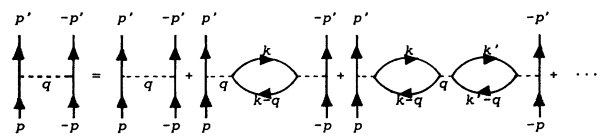

FIG. 1. The bubble diagrams of $NN\omega$ interaction.

$$\begin{aligned}\tilde{\Sigma}^{\mu\nu}_{\omega}(q,\beta,\rho) &= -ig^2_{\omega}\int\frac{d^4k}{(2\pi)^4}\mathrm{Tr}[\gamma^{\mu}\Delta_{11}(k)\gamma^{\nu}\Delta_{11}(k-q)] \\ &= -ig^2_{\omega}\int\frac{d^4k}{(2\pi)^4}\tau^{\mu\nu}\left[\frac{1}{k^2-M^2_N}\frac{1}{(k-q)^2-M^2_N}\right] \\ &\quad +2\pi g^2_{\omega}\int\frac{d^4k}{(2\pi)^4}\tau^{\mu\nu}\left(\frac{\delta(k^2-M^2_N)}{(k-q)^2-M^2_N}[\theta(k_0)n_F(k)+\theta(-k_0)\bar{n}_F(k)]\right. \\ &\quad \left.+\frac{\delta((k-q)^2-M^2_N)}{k^2-M^2_N}[\theta(k_0-q_0)n_F(k-q)+\theta(-k_0+q_0)\bar{n}_F(k-q)]\right) \\ &\equiv \Sigma^{\mu\nu}_{\omega}(q,0)+\Sigma^{\mu\nu}_{\omega}(q,\beta,\rho)\ , \end{aligned} \tag{13}$$

where

$$\begin{aligned}\tau^{\mu\nu} &= \mathrm{Tr}[\gamma^{\mu}(\not{k}+M_N)\gamma^{\nu}(\not{k}-\not{q}+M_N)] \\ &= 4\{k^{\mu}(k-q)^{\nu}+k^{\nu}(k-q)^{\mu} \\ &\quad -q^{\mu\nu}[k(k-q)-M^2_N]\}\ . \end{aligned} \tag{14}$$

$\Sigma^{\mu\nu}_{\omega}(q,0)$ is the contribution at zero temperature and density, which can be renormalized as usual in quantum field theory. Since we are interested in the temperature and density effects, from now on we only discuss the temperature- and density-dependent part $\Sigma^{\mu\nu}_{\omega}(q,\beta,\rho)$. For the low-energy $NN\omega$ nuclear interaction, under the nonrelativistic limit $|\mathbf{q}| \ll M_{\omega}$ [8–10], we have

$$\Sigma^{00}_{\omega}(q,\beta,\rho) \approx 0\ , \tag{15}$$

$$\Sigma^{ij}_{\omega}(q,\beta,\rho) = \left(g^{ij}+\frac{q^iq^j}{|\mathbf{q}|^2}\right)\Sigma_{\omega}(q,\beta,\rho)\ . \tag{16}$$

The Dyson equation at finite temperature and finite density has the same form as Eq. (9), except with the substitution of $\Sigma^{\lambda\sigma}_{\omega}(q,0)$ and $D^0_{\mu\nu}(q)$ by $\Sigma^{\lambda\sigma}_{\omega}(q,\beta,\rho)$ and the (1,1) component of the ω meson propagator matrix in TFD [17]. After some calculations, we obtain

$$D^{00}(q) = \frac{-g^{00}}{q^2-M^2_{\omega}}\ , \tag{17}$$

$$D^{ij}(q) = \frac{-g^{ij}}{q^2-M^2_{\omega}+\Sigma_{\omega}(q,\beta,\rho)} \tag{18}$$

in the nonrelativistic limit, where M_{ω} is the renormalized mass of the ω meson at zero temperature and density, and $\Sigma_{\omega}(q,\beta,\rho)$ is given by

$$\begin{aligned}\Sigma_{\omega}(q,\beta,\rho) &= \tfrac{1}{2}g_{ij}\Sigma^{ij}_{\omega}(q,\beta,\rho) \\ &= \pi g^2_{\omega}\int\frac{d^4k}{(2\pi)^4}g_{ij}\tau^{ij}\left(\frac{\delta(k^2-M^2_N)}{(k-q)^2-M^2_N}[\theta(k_0)n_k+\theta(-k_0)\bar{n}_k]\right. \\ &\quad \left.+\frac{\delta((k-q)^2-M^2_N)}{k^2-M^2_N}[\theta(k_0-q_0)n_{k-q}+\theta(-k_0+q_0)\bar{n}_{k-q}]\right)\ , \end{aligned} \tag{19}$$

where

$$g_{ij}\tau^{ij} = 4[\mathbf{k}\cdot(\mathbf{k}-\mathbf{q})-3k_0(k_0-q_0)+3M^2_N]\ . \tag{20}$$

Due to the conservation of baryon current, we have [8]

$$q_{\mu}D^{\mu\nu}(q) = q^{\nu}/M^2_{\omega}\ . \tag{21}$$

By using Eq. (21), we can prove that

$$D^{i0}(q) = D^{0i}(q) = 0 \tag{22}$$

in the nonrelativistic limit. Straightforward calculations using Eqs. (19) and (20) can give

$$\Sigma_{\omega}(q,\beta,\rho) = \frac{g^2_{\omega}}{2\pi^2}\left(2I_2-M^2_NI_{3/2}-\frac{q^2}{4}I_{3/2}\right)\ , \tag{23}$$

where

$$I_2 = \frac{1}{\beta^2}\int_0^\infty dx \frac{x^2}{\sqrt{x^2+\beta^2 M_N^2}}\left(\frac{1}{\exp(\sqrt{x^2+\beta^2 M_N^2}+\beta\mu)+1}+\frac{1}{\exp(\sqrt{x^2+\beta^2 M_N^2}-\beta\mu)+1}\right), \tag{24a}$$

$$I_{3/2} = \int_0^\infty dx \frac{x^2}{(x^2+\beta^2 M_N^2)^{3/2}}\left(\frac{1}{\exp(\sqrt{x^2+\beta^2 M_N^2}+\beta\mu)+1}+\frac{1}{\exp(\sqrt{x^2+\beta^2 M_N^2}-\beta\mu)+1}\right). \tag{24b}$$

Substituting Eqs. (23) and (24) into Eq. (18), we finally obtain

$$D^{ij}(q) = H^2 \frac{-g^{ij}}{q^2 - M_\omega^{*2}}, \tag{25}$$

where

$$H = \left(1 - \frac{g_\omega^2}{4\pi^2} I_{3/2}\right)^{-1/2} \tag{26}$$

and

$$M_\omega^* = H\left(M_\omega^2 - \frac{g_\omega^2}{2\pi^2}(2I_2 - M_N^2 I_{3/2})\right)^{1/2} \tag{27}$$

is the effective mass of the ω meson at finite temperature and finite density. We will use it to check the Brown-Rho conjecture in Sec. III.

C. One-omega-exchange potential

Following similar treatments to those of our previous works [7–10], the finite-temperature and finite-density effective one-omega-exchange potential (OOEP) can now be found as

$$V_\omega(r) = \frac{g_\omega^2}{4\pi} M_\omega \left[\left(1+\frac{M_\omega^2}{4M_N^2}\right)Y(x') + \frac{M_\omega^2}{2M_N^2}\mathbf{S}\cdot\mathbf{L}\frac{1}{x'}\frac{dY(x')}{dx'}\right]$$
$$+\frac{g_\omega^2 H^2}{4\pi} M_\omega^* \left(\frac{M_\omega^{*2}}{4M_N^2}Y(x) + \frac{M_\omega^{*2}}{2M_N^2}\mathbf{S}\cdot\mathbf{L}\frac{1}{x}\frac{dY(x)}{dx} - \frac{1}{12}\frac{M_\omega^{*2}}{M_N^2}[Z(x)S_{12} + Y(x)(\boldsymbol{\sigma}_1\cdot\boldsymbol{\sigma}_2)] + \frac{1}{4}\frac{M_\omega^{*2}}{M_N^2}Y(x)(\boldsymbol{\sigma}_1\cdot\boldsymbol{\sigma}_2)\right), \tag{28}$$

where

$$x' = M_\omega r, \quad x = M_\omega^* r, \quad Y(x) = e^{-x}/x,$$

$$Z(x) = \left(1+\frac{3}{x}+\frac{3}{x^2}\right)Y(x), \tag{29}$$

$$S_{12} = \frac{3(\boldsymbol{\sigma}_1\cdot\mathbf{r})(\boldsymbol{\sigma}_2\cdot\mathbf{r})}{r^2} - \boldsymbol{\sigma}_1\cdot\boldsymbol{\sigma}_2.$$

Obviously, Eq. (28) has a similar form as in the naive nuclear theory [18]. The numerical results for OOEP will be shown in the next section.

III. RESULTS AND DISCUSSIONS

The finite-temperature and finite-density effective OOEP and the effective mass of ω meson can be calculated numerically from Eqs. (23) and (24), (26) and (27), and (28) and (29). Our results from numerical computation are shown in Figs. 2–6.

Figure 2 shows the temperature dependence of M_ω^*/M_ω for a density $\rho = 0.100$ fm^{-3}, where the solid curve represents the results given by our formulas. The parameters $M_N = 983.3$ MeV, $M_\omega = 782.6$ MeV, and $g_\omega = 15.85$ have been chosen as in Ref. [19]. In order to compare our results with those given by Eqs. (1) and (2), we define an error function Δ_e as

$$\Delta_e = \left[\frac{1}{N}\sum_i (M_i - M_{i0})^2\right]^{1/2}, \tag{30}$$

where N is the number of match points, M_i and M_{i0} are the values of M_ω^*/M_ω given by our formulas and by Eq. (2), respectively. We choose $N = 24$ and adjust the parameter n in Eq. (2) to get a best fit with the restriction that $\Delta_e \lesssim 10^{-2}$. The dashed curve in Fig. 2 shows the results given by Eq. (2) where $n = 0.21$ and

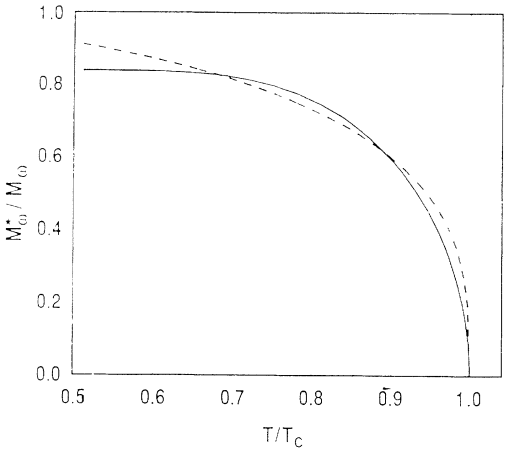

FIG. 2. The temperature dependence of M^*_ω/M_ω for $\rho = 0.100$ fm^{-3}, where the solid line is given by our formulas and the dashed line by Eq. (2). The parameters chosen are $n = 0.21$ and $T_c = 335.6$ MeV.

$T_c = 335.62$ MeV. The cases for $\rho = 2\rho_0 = 0.34$ fm^{-3}, where ρ_0 is the saturation density, are similarly plotted in Fig. 3, in which $n = 0.31$ and $T_c = 333.03$ MeV. From Fig. 3, we see that we also obtain a best fit between our formulas and Eqs. (1) and (2) for $\rho = 2\rho_0$.

To check the Brown-Rho conjecture in a wider density range, we calculate M^*_ω/M_ω using our formulas and fit the value given by Eq. (2) for different densities. The results are shown in Table I. We see that Eqs. (1) and (2) can satisfactorily describe M^*_ω/M_ω in the low-density region. However, n is a monotonously increasing function and T_c at which M^*_ω equals to zero is a monotonously decreasing function of ρ. As the density increases, Δ_e increases. This means that the fit by Eq. (2) becomes poorer as the density increases. When $\rho > 4\rho_0$, the fit is unsatisfactory. For example, the plot of M^*_ω/M_ω with T/T_c shown in Fig. 4 where $n = 0.61$ and $T_c = 305.6$ MeV has $\Delta_e = 18.13 \times 10^{-2}$ given by our formulas and by the Brown-Rho conjecture for $\rho = 0.94$ fm^{-3}, and there

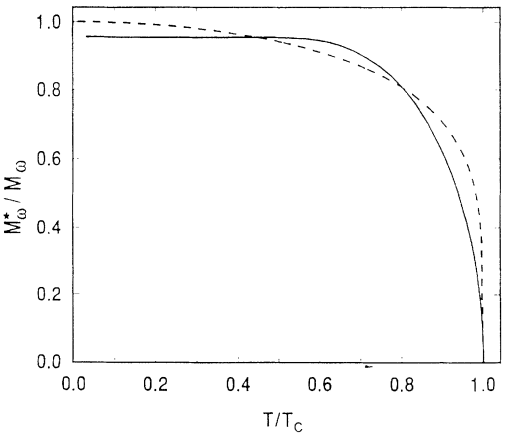

FIG. 3. The temperature dependence of M^*_ω/M_ω for $\rho = 0.340$ fm^{-3}, where the solid line is given by our formulas and the dashed line by Eq. (2). The parameters chosen are $n = 0.31$ and $T_c = 333.0$ MeV.

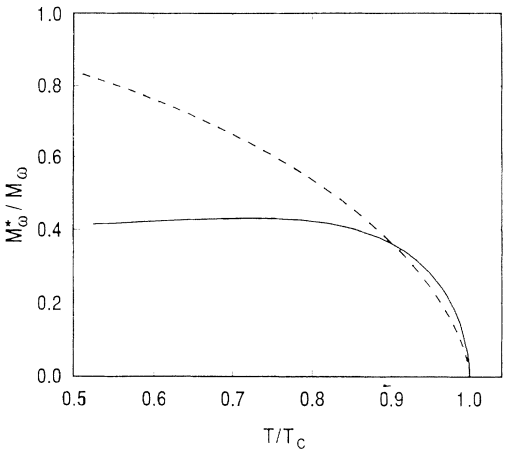

FIG. 4. The temperature dependence of M^*_ω/M_ω for $\rho = 0.940$ fm^{-3}, where the solid line is given by our formulas and the dashed line by Eq. (2). The parameters chosen are $n = 0.61$ and $T_c = 305.6$ MeV.

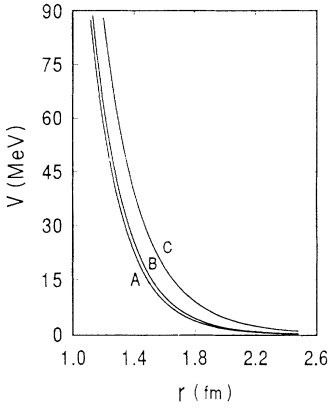

FIG. 5. The effective OOEP curves for different temperatures. A: $T = 10$ MeV; B: $T = 250$ MeV; C: $T = 300$ MeV. The density is fixed at $\rho = 0.17$ fm^{-3}.

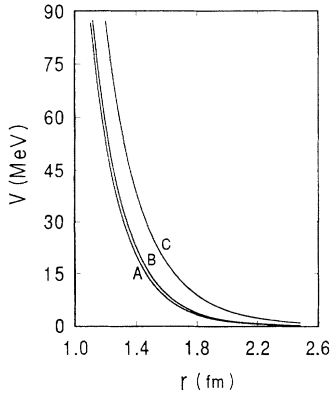

FIG. 6. The effective OOEP curves for different densities. A: $\rho = 0.006$ fm^{-3}; B: $\rho = 0.170$ fm^{-3}; C: $\rho = 0.680$ fm^{-3}. The temperature is fixed at $T = 10$ MeV.

is a considerable discrepancy between the solid curve and the dashed curve, especially in the low-temperature region.

The effective OOEP curves for various temperatures are shown in Fig. 5 where we have fixed $\rho = 0.17$ fm^{-3}. The curves A, B, and C correspond to $T = 10$, 250, and 300 MeV, respectively. We see that the repulsive cores for nuclear force become harder as the temperature increases, which is, of course, very reasonable.

The effective OOEP curves for a fixed temperature $T = 10$ MeV and for different densities are shown in Fig. 6, where the curves A, B, and C refer to $\rho = 0.006$, 0.170, and 0.600 fm^{-3}, respectively. We see that the repulsive cores for the nuclear force become harder as the density increases. In fact, the density plays the same role as the temperature [7].

In summary, we would like to point out that the influence of temperature and density are very important on OOEP as well as on the effective mass of ω meson. Based on the thermofield dynamic theory, and considering vacuum polarization, we find that the formula for the effective mass of the ρ meson can also be used to describe the ω meson in the low-density region ($\rho \lesssim 4\rho_0$), but since the parameter n and T_c all depend on the density, the Brown-Rho conjecture seems to fail in the high-density region ($\rho > 4\rho_0$).

TABLE I. The parameters n, T_c, and the corresponding error function Δ_e for describing M^*_ω/M_ω by Eq. (2) at various densities.

ρ (fm^{-3})	n	T_c (MeV)	Δ_e
0.006	0.194	335.9	2.38×10^{-2}
0.100	0.210	335.6	2.56×10^{-2}
0.170	0.260	335.2	3.55×10^{-2}
0.340	0.310	333.0	5.12×10^{-2}
0.680	0.460	323.1	9.50×10^{-2}

This work was supported in part by the National Science Foundation of China under Grant No. 19175014, and by the Foundation of State Education Commission of China.

[1] G. E. Brown, Nucl. Phys. **A522**, 397c (1991); **A488**, 695c (1988); Z. Phys. C **38**, 291 (1988).
[2] G. E. Brown and M. Rho, Phys. Rev. Lett. **66**, 2720 (1991).
[3] T. Hatsuda and T. Kunihiro, Phys. Lett. B **185**, 304 (1987).
[4] V. Bernard, U. Meissner, and I. Zahed, Phys. Rev. D **36**, 819 (1987).
[5] M. P. Allendes and B. D. Serot, Phys. Rev. C **45**, 2975 (1992).
[6] S. Weinberg, Nucl. Phys. **B363**, 3 (1991); Phys. Lett. B **251**, 288 (1990).
[7] Z. X. Qian, C. G. Su, and R. K. Su, Phys. Rev. C **47**, 877 (1993).
[8] R. K. Su, Z. X. Qian, and G. T. Zheng, J. Phys. G **17**, 1785 (1991).
[9] R. K. Su and G. T. Zheng, J. Phys. G **16**, 1861 (1990).
[10] R. K. Su, G. T. Zheng, and G. G. Siu, J. Phys. G **19**, 79 (1993).
[11] R. K. Su, S. D. Yang, and T. T. S. Kuo, Phys. Rev. C **35**, 1539 (1987).
[12] H. Q. Song and R. K. Su, Phys. Rev. C **44**, 2505 (1991).
[13] H. Umezawa, H. Matsumoto, and M. Tachiki, *Thermo Field Dynamics and Condensed Matter* (North-Holland, Amsterdam, 1982).
[14] Y. Fujimoto, Phys. Lett. **141B**, 83 (1984).
[15] K. Kusaka and W. Weise, Phys. Lett. B **288**, 6 (1992).
[16] T. Hatsuda and S. H. Lee, Phys. Rev. C **46**, R34 (1992).
[17] R. L. Kobes and G. W. Semenoff, Nucl. Phys. **B260**, 714 (1985).
[18] R. K. Su and E. M. Henley, Nucl. Phys. **A452**, 633 (1986).
[19] R. Machleidt, K. Holinde, and Chelster, Phys. Rep. **149**, 1 (1987).